Electronic Supplementary Information:

Electrochemical Li^+ Insertion Capability into $Na_{4-x}Co_3(PO_4)_2P_2O_7$ and Its Application to Novel Hybrid-ion Battery

Masafumi Nose,[a] Kunihiro Nobuhara,[a] Shinya Shiotani,[b] Hideki Nakayama,[a] Shinji Nakanishi[a] and Hideki Iba[a]

[a]*Toyota Motor Corporation, Battery Research Division, 1200 Mishuku, Susono, Shizuoka 410-1193, Japan.*
E-mail: nose@masafumi.tec.toyota.co.jp
[b]*Toyota Motor Corporation, Material Development Management Division, 1 Toyota-cho, Toyota, Aichi、471-8572, Japan.*

Electrode preparation and characterization of as-prepared material

$Na_4Co_3(PO_4)_2P_2O_7$ was prepared by sol-gel method and subsequently heat treatment. The stoichiometric ratio (Na : Co : P = 40 : 30 : 40 mmol) of $(CH_3COO)_2Co$, $Na_4P_2O_7$ and $NH_4H_2PO_4$ (Nacali tesque) was dissolved into 2 $moldm^{-3}$ HNO_3 solution (190 mL) and then glycolic acid (16 g) was added to prevent the particle growth. The solution was heated at 80°C for 12hr with continuous stirring. The gel was annealed at 680°C for 50hr under air atmosphere. The powder and Vapor-Grown Carbon Fiber (Showa Denko, VGCF) were mixed with a weight ratio of 5 to 1, and heat treatment was carried out at 680°C for 5hr under purging Ar. Then, a N-methyl pyrrolidone based slurry composed of the mixture of $Na_4Co_3(PO_4)_2P_2O_7$ (75 wt%) and VGCF (15 wt%), acetylene black (5 wt%) as a conductive filler and poly(vinylidene fluoride) (5 wt%) as a binder was cast on an aluminum current collector.

The as-prepared electrode material as described above was characterized by synchrotron X-ray diffraction measurement at beam line BL19B2 SPring-8 in Japan. The wavelength of incident X-ray beam was set to 0.5Å using a silicon monochromator. Structural analysis was carried out by Rietveld analysis using RITEN-FP. [1)]

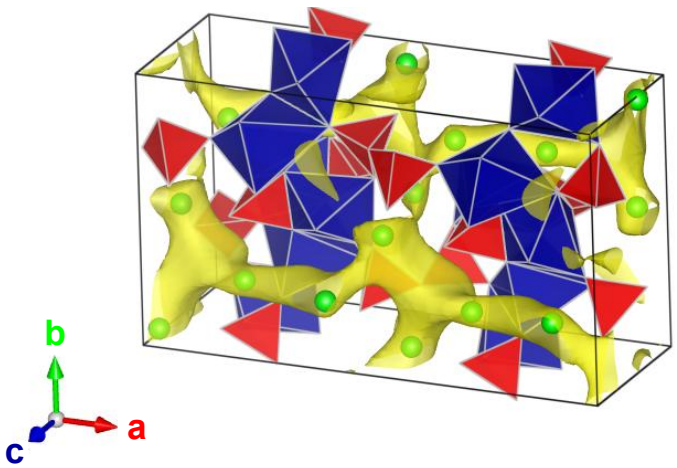

Figure S1 Polyhedral view[2)] of $Na_4Co_3(PO_4)_2P_2O_7$ and diffusion pathways visualized by bond valence sum (BVS) method.

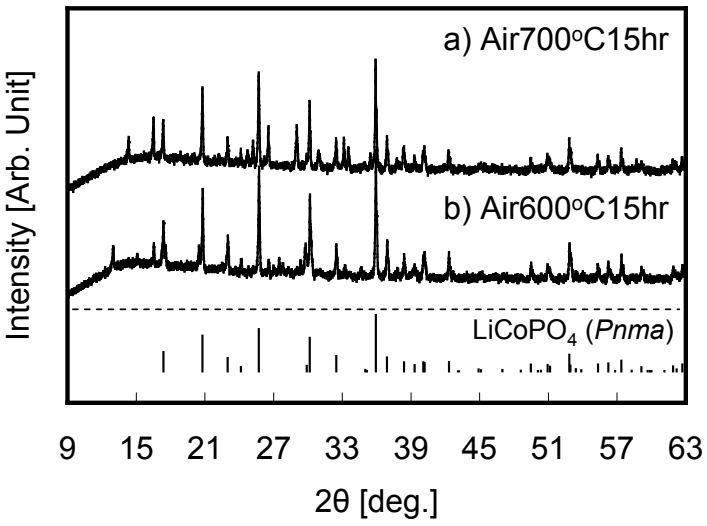

Figure S2 XRD patterns of as-prepared materials by sol-gel method and heat treatment at a) 600°C and b) 700°C for 15hr under air atmosphere.

To synthesize novel phase $Li_4Co_3(PO_4)_2P_2O_7$ (Space group : *Pna*2_1), stoichiometric ratio (Li : Co : P = 4 : 3 : 4) of CH_3COOLi , $(CH_3COO)_2Co$ and $NH_4H_2PO_4$ (Nacali tesque) was dissolved into a diluted nitric acid solution and then glycolic acid was added to prevent the particle growth. The solution was heated at 80°C for 12hr with continuous stirring. Then, the gel was annealed at 600°C or 700°C for 15hr under air atmosphere. As shown in Fig. S2, main diffraction peaks obtained by XRD measurements were indicated as $LiCoPO_4$ (*Pnma*).

Generally, some sodium-based compounds such as Na_2FePO_4F are not familiar with lithium equivalences because more stable compounds (i.e. $LiMPO_4$ and LiF) were produced.[3] Also, it is too difficult to prepare olivine-phase $NaMPO_4$ by direct synthesize, while some reports successfully obtained olivine-phase $NaFePO_4$ by ion exchange of olivine-phase $LiFePO_4$.[4, 5] As is well known, maricite-phase $NaMPO_4$ was obtained by direct synthesis. These results indicate thermodynamically stable compounds and/or crystal structure of sodium-based compounds can not be similar to those of lithium counterparts.

One of the reasons for the difference of stable phases or crystal structure would be derived from the wide gap of ionic radii between Na^+ (102 pm) and Li^+ (76 pm). In the case of $Li_4Co_3(PO_4)_2P_2O_7$ (Space group : *Pna*2_1), $LiCoPO_4$ (*Pnma*) as a more stable phase than $Li_4Co_3(PO_4)_2P_2O_7$ was indicated as a main product by the current sol-gel method. $Li_4Co_3(PO_4)_2P_2O_7$ might exist as a meta-stable phase, for example, at lower or higher temperatures. Also, $Li_4Co_3(PO_4)_2P_2O_7$ might be obtained by ionic exchange of Na^+ in $Na_4Co_3(PO_4)_2P_2O_7$. But unfortunately, we could not find the meta-stable phase of $Li_4Co_3(PO_4)_2P_2O_7$ by using the direct synthesis as described in this manuscript.

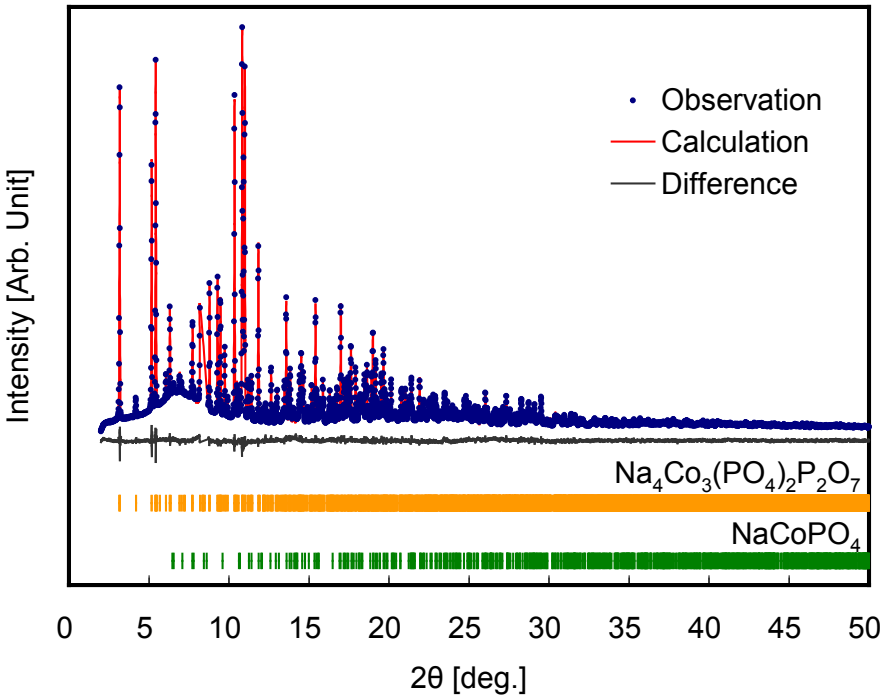

Figure S3 Synchrotron X-ray diffraction pattern with Rietveld refinement.

Figure S3 shows the synchrotron X-ray diffraction and Rietveld refinement patterns of as-prepared material. A small trace (ca. 3 wt.%) of $NaCoPO_4$ was identified as impurity and the crystal structure of the main product (ca. 97 wt.%) was successfully indexed with space group $Pna2_1$ in an orthorhombic unit cell. The fitting was satisfactory (R_{wp}=4.65, R_e=4.12 and S=1.13).

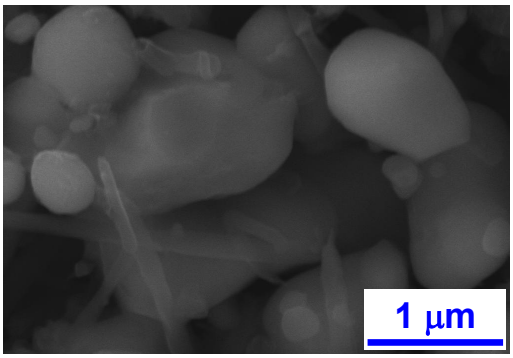

Figure S4 FE-SEM images of Na4Co3(PO4)2P2O7/VGCF composite.

Figure S4 shows the surface morphology of $Na_4Co_3(PO_4)_2P_2O_7$ / VGCF composite obtained by using FE-SEM (Ultra55, ZEISS). The image revealed the particle size ranges roughly from 300 nm to 3 μm.

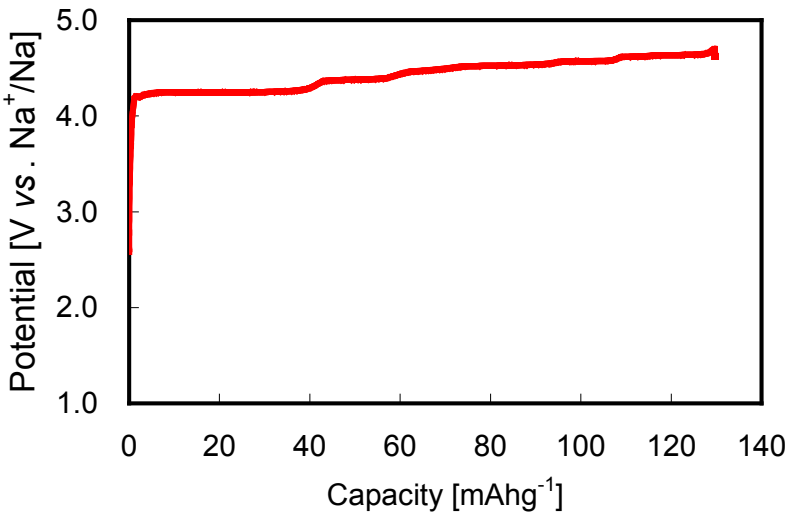

Figure S5 Charge profile of $Na_4Co_3(PO_4)_2P_2O_7$ at 34 mAg^{-1} (0.2C) up to 4.7 V *vs*. Na^+/Na in 1.0 $moldm^{-3}$ $NaPF_6$ in EC/DEC [50 : 50 by vol. %].

Figure S5 shows 1st charge profile of $Na_4Co_3(PO_4)_2P_2O_7$ at the current density of 34 mAg^{-1} (0.2C rate) by using Na metal as a counter electrode. As reported in our previous paper, $Na_4Co_3(PO_4)_2P_2O_7$ has multi-redox couples in the wide potential region of 4.1 V and 4.7 V vs. Na^+/Na.[6] Hence, Co^{2+} in $Na_4Co_3(PO_4)_2P_2O_7$ is gradually oxidized close to Co^{3+} at 4.7 V vs. Na^+/Na *via*. intermediate valence states in each redox couples. The complex multi-redox behavior would be derived from a variety of Na^+ sites in the crystal structure and/or Na^+-ordering during Na^+ extraction/insertion, which could affect operating potential *vs*. Na^+ contents in $Na_{4-x}Co_3(PO_4)_2P_2O_7$. In other words, while Na^+ extraction from $Na_4Co_3(PO_4)_2P_2O_7$ operated at around 4.2 V vs. Na^+/Na which corresponds to the low potential plateau region around 4.2 V, further Na^+ extraction from partially Na^+-extracted $Na_{4-x}Co_3(PO_4)_2P_2O_7$ operated at higher potential region above 4.2 V vs. Na^+/Na. The highest redox potential of $Na_{4-x}Co_3(PO_4)_2P_2O_7$ reached up to ca. 4.6 V vs. Na^+/Na, which corresponds to ca. 4.9 V *vs*. Li^+/Li and is almost the same as the operating potentials of lithium-based cobalt phosphates such as $LiCoPO_4$, Li_2CoPO_4F and $Li_2CoP_2O_7$.[7-9]

Next, Na^+-extracted $Na_{1.4}Co_3(PO_4)_2P_2O_7$ shows nearly identical open circuit potentials (OCV) of 4.6 V *vs*. Na^+/Na and 4.8 V *vs*. Li^+/Li in sodium and lithium-based electrolytes, respectively. But, as shown in Fig. 1, polarizations ($\Delta E/V$) of Li^+ insertion at higher rates were apparently larger than those of Na^+ insertion at the same rates and therefore Li^+ insertion potentials especially at higher rates was lower than Na^+ insertion potentials. Polarization in rocking-chair type battery system should be dependent on kinetics of bulk diffusivity and ion transport at the interface between electrolyte and electrode. Regarding bulk diffusivity, Li^+ insertion into $Na_{1.4}Co_3(PO_4)_2P_2O_7$ suffered from the disadvantages such as structural distortion with anisotropic volume change, which

could affect lower diffusivity than Na^+ insertion. On the other hand, Na^+ transport at the interface is generally considered faster than Li^+ insertion because of lower Lewis acidity of Na^+ than Li^+ and therefore lower desolvation energy of Na^+-solvent than Li^+-solvent. These behaviors support lower polarization of Na^+ insertion than Li^+ insertion, which leads to higher discharge potential of Na^+ insertion than Li^+ insertion.

Finally, typical $NaPF_6$ based organic electrolytes as used in this paper can be unstable for oxidation decomposition at such a high potential of 4.7 V vs. Na^+/Na, corresponding to 5.0 V vs. Li^+/Li. As discussed in the manuscript, 2.6 Na^+ in $Na_4Co_3(PO_4)_2P_2O_7$, which corresponds to ca. 115 $mAhg^{-1}$, could be extracted by charge reaction. But actually, the charge capacity reached to 130 $mAhg^{-1}$, as described in Fig. S5. The extra charge capacity of ca. 15 $mAhg^{-1}$ indicates irreversible oxidation of the $NaPF_6$ electrolyte should occur. The decomposition of the electrolyte especially at first charge reaction is one of the most serious issues to be solved before the commercialization of Na ion battery and further investigation of the electrolyte with wide potential window will be desired.

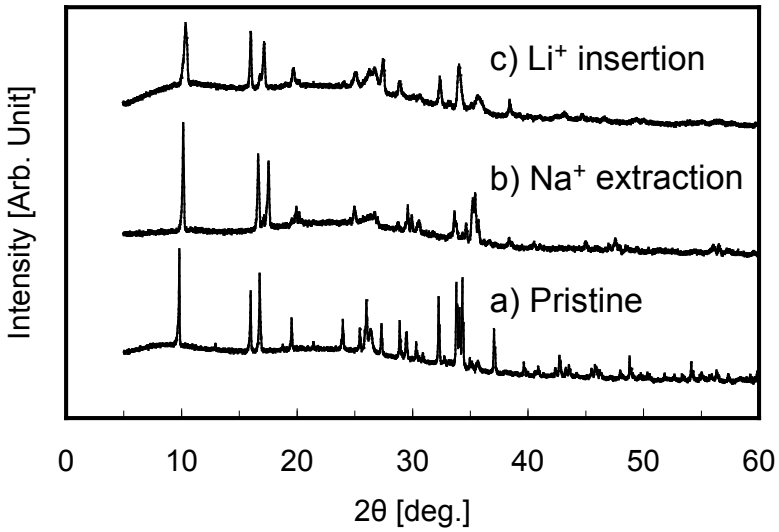

Figure S6 *ex-situ* XRD patterns of a) as-prepared, b) Na^+ extracted and c) Li^+ inserted electrode materials.

The XRD patterns of the pristine, Na^+-extracted and Li^+-inserted electrodes directly reflects the changes of the crystal structure and lattice constant by Na^+ extraction and then Li^+ insertion. Main reasons for these changes should be ascribed as the differences of ionic radii not only between Co^{2+} and Co^{3+} but also between Na^+ and Li^+. When Na^+ was extracted from $Na_4Co_3(PO_4)_2P_2O_7$ by charge reaction, the change of ionic radii of Co^{2+}/Co^{3+} and therefore the changes of the bond length between Co^{2+} and O^{2-} can dominantly contribute to the changes of the XRD patterns. Regarding the comparison of the pristine and Li^+ inserted electrodes, the differences of ionic radii between Na^+ and Li^+ should play an important role in the changes of the crystal structure and/or lattice constant because of almost the same valence state of Co ion. Actually, Li^+ occupancy sites can not be refined by Rietveld analysis of the Li^+ inserted structure, which would be desired to discuss the Li^+ insertion mechanism in more detail. Nevertheless, significant peak shifts on the XRD patterns bring us valuable information on Li^+ insertion mechanism. This is the reason why we discuss the Li^+ insertion mechanism from the standpoint of the shrinkage and expansion of some lattice planes which were clearly changed by Na^+ extraction and then Li^+ insertion. Additionally, some peaks at 33-37^o clearly shifted during charge/discharge and some of them disappeared by Na^+ extraction or new peaks appeared by Li^+ insertion. But unfortunately, these shifts of peak positions at each diffraction patterns can not be distinguished, because the XRD pattern of the pristine electrode contains so many diffraction patterns at 33-37^o because of the low symmetry of the crystal structure. Actually, these patterns roughly tend to shift to higher positions by Na^+ extraction and then lower positions by Li^+ insertion, which can be similar behavior to (011) and (210) planes.

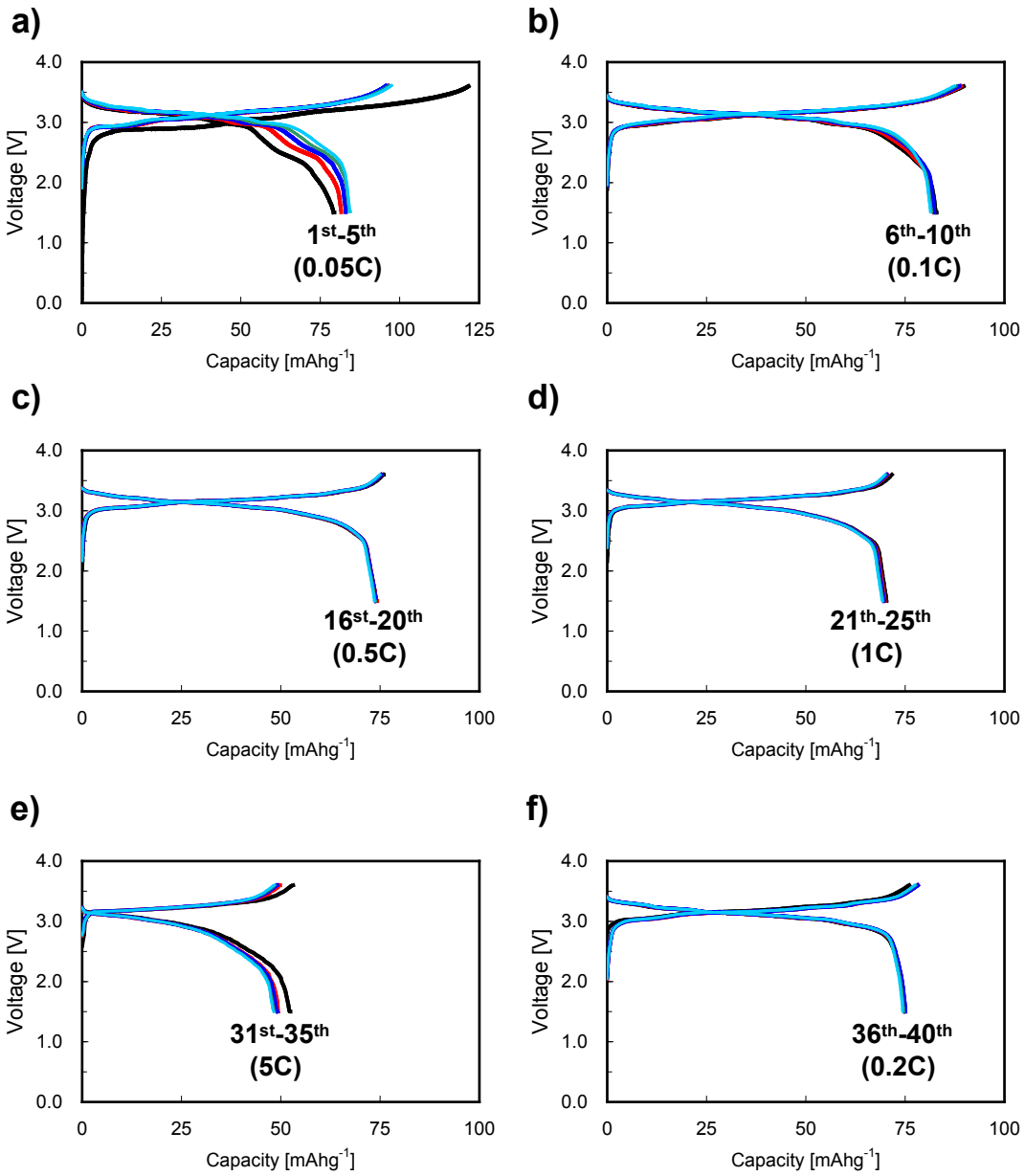

Figure S7 Charge/discharge profiles of the new HIB at a) 1-5 cycles (0.05C), b) 6-10 cycles (0.1C), c) 16-20 cycles (0.5C), d) 21-25 cycles (1C), 31-35 cycles (5C) and 36-40 cycles (0.2C).

References

1. F. Isumi and K. Momma, *Solid state Phenomena*, 2007, **130,** 15-20.

2. K. Momma and F. Izumi, *J. Applied Crystallography*, 2008, **41,** 653-658.

3. J.-M. Tarascon, N. Recham, M. Armand, J.-N. Chotard, P. Barpanda, W. Walker and L. Dupont, *Chem. Mater.*, 2010, **22,** 724-739.

4. K. Zaghiba, J. Trottier, P. Hovington, F. Brochu, A. Guerfi, A. Mauger and C. M. Julien, *J. Power Sources*, 2011, **196,** 9612– 9617.

5. S.-M. Oh, S.-T. Myung, J. Hassoun, B. Scrosati and Y.-K. Sun, *Electrochem. Comm.*, 2012, **22,** 149–152.

6. M. Nose, H. Nakayama, K. Nobuhara, H. Yamaguchi, S. Nakanishi and H. Hideki, *J. Power Sources*, 2013, **234,** 175-179.

7. S. Okada, M. Ueno, Y. Uebou and J. Yamaki, *J. Power Sources*, 2005, ***146,*** 565-569.

8. H. Kim, S. Lee, Y.-U. Park, H. Kim, J. Kim, S. Jeon and K. Kang, *Chem. Mater.,* 2011, **23,** 3930-3937.

9. S. Okada, S. Sawa, M. Egashira, J. Yamaki, M. Tabuchi, H. Kageyama, T. Konishi and A. Yoshino, *J. Power Sources*, 2011, ***97–98,*** 430-432.

Acknowledgement

We would like to thank Prof. M. Nakayama (Nagoya Institute of Technology, Department of Materials Science and Engineering) for his technical supports to visualize diffusion pathways in the crystal structure of $Na_4Co_3(PO_4)_2P_2O_7$ by using BVS method.